ce/papers Proceedings in civil engineering

Ernst & Sohn A Wiley Brand

ORIGINAL ARTICLE

ibausil
F.A. Finger-Institut für Baustoffkunde
Bauhaus-Universität Weimar

Investigation of a hybrid binder system for large scale 3D printing

Sebastian Remke[1] | Gaurav Sant[2,3,4,5] | Torben Gädt[1]

Correspondence

Prof. Dr. Torben Gädt
Technical University of Munich
TUM School of Natural Science
Lichtenbergstraße 4
85748 Garching
Email: torben.gaedt@tum.de

[1] Technical University of Munich, TUM School of Natural Science, Chemistry of Construction Materials
[2] University of California Los Angeles, Department of Civil and Environmental Engineering, Laboratory for the Chemistry of Construction Materials (LC²)
[3] University of California Los Angeles, Institute for Carbon Management (ICM)
[4] University of California Los Angeles, California Nanosystems Institute (CNSI)
[5] University of California Los Angeles, Department of Materials Science and Engineering

Abstract

Large-scale additive manufacturing of reactive suspensions, such as concrete, is being developed to freely create objects without the constraints of a formwork. One challenge in printing suspensions is the precise spatio-temporal control over their rheological properties. For extrusion-based processes the material must be pumpable to the nozzle of the printer, while once it has passed the nozzle, it must maintain its shape under the increasing pressure of subsequent layers. Therefore, it is beneficial if the material exhibits an appropriately designed rheology change at the nozzle. The objective of this work is to develop a printing suspension which achieves a rheological step change at the nozzle. Therefore, we create a hybrid binder system comprising of a fast, reactive organic component, which can be activated by heat and a second inorganic binder components, in our system the carbonation of calcium hydroxide, which delivers the final strength.

The temperature dependent stiffening of the model suspensions is studied by oscillatory rheology at temperatures between 20 °C to 80 °C. For mechanical testing purposes, cuboid shaped samples are obtained by microwave heating followed by carbonation under ambient conditions. For the given porosity, the material reaches a compressive strength of up to 0.39 MPa in 10 seconds or up to 1.94 MPa in 10 minutes depending on the heating program. Subsequent carbonation for 7 days under ambient conditions gives a strength of up to 4.76 MPa.

Keywords

3D-Printing, Rheology, Polymer, Carbonation, Compressive Strength, Acrylic Acid, Calcium Hydroxide, Active Stiffening Control, Microwave Heating

1 Introduction

Large scale 3D-printing processes based on granular suspensions (such as concrete) have seen a rapid evolution, especially within the last few years [1–3]. The absence of a formwork, in processes like layer-based extrusion, requires a well-controlled structural build-up of the deposited suspension [4,5]. This is currently a limiting factor concerning building speed and height. In this context, materials whose rheological properties can be actively controlled are an active field of research [1,6].

Systems that include active rheology control are found in 3D printing technologies based on organic binders. Stereolithography is a photopolymerization based layer-by-layer 3D printing technology. It requires a transparent resin and objects are printed by selectively polymerizing the resin with a UV laser. This allows for a high spatial resolution, but the necessity to create objects in a resin bath limit this technology to the centimetre scale [7–9]. Larger objects can be printed by fused deposition modeling. But since this process relies on fast melting and solidification of the polymer, the nozzle diameter is limited which, together with mechanical strength and thermal degradation challenges, restricts the size of the printed objects [10,11].

3D printing techniques based on organic binders often have good to excellent spatio-temporal control over the rheological and elastic properties but are limited with regard to the scale of the resulting objects. A possible way to bring active rheology control to the large scale of construction materials could therefore be the combination of an organic binder with an inorganic suspension. Hybrid organic and inorganic binders are already studied and brought into practice [12–15]. One example from the building industry are cementitious tile adhesives which can contain significant amounts of polymer emulsions as secondary organic binder [16]. In Macro-defect-free cements the combination of organic and inorganic binder leads to improved characteristics [17]. More recently Liang et al.

used the in-situ polymerization of acryl amide in cement paste to achieve increased flexural strength [18].

A hybrid binder system which focuses on 3D printing applications was reported by Kandy et al. [19]. They used a thermally triggered epoxy-thiol condensation reaction in a mineral suspension to accomplish a very fast liquid-to-solid transition. The determination of the storage modulus during hardening revealed stiffening rates on the order of 400 Pa/s after the polymerization started.

In this study we show a similar system which avoids the use of potentially harmful chemicals. The developed suspension is based on the radical polymerization of acrylic acid in the presence of a crosslinker to achieve a fast strength build-up. Radical polymerization as polymerization process was chosen because it is fast, compatible with water, and has a good tolerance towards impurities and inhibitors [20,21]. In addition to acrylic acid and crosslinker, the suspensions contain water as continuous phase and calcium hydroxide as the inorganic binder component. Carbonation (and drying) of the material leads to a build-up of mechanical strength through the transformation of calcium hydroxide to calcite [22–24] and water loss.

1 Materials and methods

1.1 Materials

Acrylic acid (98%, stabilised) was purchased from Acros Organics, ethylene glycol dimethacrylate (98%, stabilised) was purchased from Thermoscientific, 2,2'-azobis[2-(2-imidazolin-2-yl)propan]dihydrochloride (VA-044) was obtained from Fuujifilm and calcium hydroxide (96%) was purchased from Carl Roth. All chemicals were used as received. Only deionised water was used.

1.2 Preparation of aqueous suspensions

Four pastes containing 10 (M10), 5 (M5) 2.5 (M2.5) and 0 (M0) volume percent acrylic acid were prepared. The molar ratio of initiator (VA-044, 0.5 mol%) and crosslinker (ethylene glycol dimethacrylate, 1 mol%) to acrylic acid were kept constant. The water content was adjusted to keep the volume fraction of calcium hydroxide at 40 volume percentage. The exact composition of the different suspensions is given in Table 1.

During mixing of the suspensions, ethylene glycol dimethacrylate, acrylic acid, and all but 1 mL water were mixed in a stainless-steel beaker with a four-blade mixer (IKA Eurostar 20) at 600 rpm for 10 seconds. Afterwards, calcium hydroxide was added, and the suspension was stirred for another 10 seconds at 600 rpm. The partial dissolution of calcium hydroxide leads to an increase in temperature. Therefore, the samples were cooled down in a water bath to room temperature before addition of the initiator. After approx. 5 minutes, VA-044 dissolved in 1 mL water was added to the steel beaker containing the cooled suspension and the mixture was homogenized for 1 minute at 600 rpm.

Table 1 Compositions of the used suspensions.

Name	M10	M5	M2.5	M0
Water [g]	15.00	15.50	17.25	18.00
Calcium hydroxide [g]	26.88	26.88	26.88	26.88
Acrylic acid [g]	3.15	1.58	0.79	0
Ethylenglycol dimethacrylat [mg]	87	43	22	0
VA-044 [mg]	71	35	18	0

1.3 Rheology measurements

The rheology of the pastes was measured on an Anton Paar MCR302e rheometer with a parallel plate (diameter = 25 mm) setup. The distance between the plates was fixed to 1 mm. To avoid water evaporation a solvent trap was used and Serva silicon oil DC 200, 350 cst was used to seal the gap between the plates. The evolution of the storage modulus was determined using a small amplitude shear (SAOS) protocol at increasing temperatures.

To eliminate shear history effects all suspensions were pre-sheared for 60 seconds with an increasing rotational speed, ramping linear from 1 to 10 s^{-1}, before oscillating at 1 Hz with an amplitude of 0.01% for 60 seconds. Then the oscillatory measurements over the temperature ramp (20°C to 80°C) were performed at a fixed frequency of 1 Hz and a fixed strain of 0.1%. To ensure a uniform temperature and minimize thermal lag, the heating rate was set to 2°C/min.

1.4 Microwave treatment

Rectangular cuboids (15 * 15 * 10 mm) were prepared by filling the suspension in a silicone mould for 9 cuboids. After filling the mould halfway, the mould was placed on a glass plate and the vibration of a vortex mixer (Merck Eurolab MELB1719) was used for compaction. Then the mould was filled completely, and excess paste was removed with a spatula. For heating, a household appliance microwave instrument was used (Panasonic NN-SD27HSGTG).

Two heating programs (Table 2) were used. For P1 the silicon mould was placed directly in the microwave. For P2 the silicon mould was placed in a two-liter crystallisation dish with a diameter of 19 cm. The dish was filled with 200 mL water, leaving the silicon mould almost submerged while avoiding surface coverage of the cuboids. The whole assembly i.e., water bath plus mould, was then placed in the microwave.

Table 2 Conditions of the microwave programs.

Program	Time [s]	Power [W]	Water bath
P1	10	1000	No
P2	600	100	Yes

1.5 Compressive strength tests

The compressive strength of all evaluated specimen was measured on a 20 kN universal testing machine (Inspect Blue from Hegewald & Peschke). As advised in DIN EN ISO 604 the longest side of the cuboid (15 mm) was placed parallel and the smallest cross section (10*15 mm) perpendicular to the axis of the compression force. The dimensions and weight of each rectangular cuboid were measured before testing. One measurement series consisted of 9 cuboids. If the compressive strength of one cuboid differed more than 50% from the mean value of the series the sample was excluded from the data. If more than three cuboids in on series failed, the whole measurement was repeated.

2 Results and discussion

2.1 Thermomechanical behaviour

The thermomechanical behaviour of the different mixes was measured by small amplitude oscillation measurements at increasing temperatures (Figure 1). Even before increasing the temperature the storage modulus of M0 differs significantly from the mixtures containing acrylic acid. This implies that acrylic acid has a dispersing effect. Such dispersing effects are also reported for other small organic molecules in mineral suspensions [25]. Most likely, acrylic acid adsorbs on the surface of the calcium hydroxide particles and leads to a negative surface potential of increased magnitude. Assuming that the adsorption of acrylic acid is the cause of the dispersing effect, one can explain the decrease of the storage modulus from M0 to M2.5 to M5. More acrylic acid leads to the increase in magnitude of the surface potential due to a higher surface coverage. The almost identical storage modulus of M5 and M10 is tentatively ascribed to complete surface coverage in M5, making further addition of acrylic acid ineffective.

All mixtures, including M0, have a constant increase of the storage modulus with temperature. Since M0 does not contain acrylic acid, this effect cannot depend on the presence of acrylic acid. The behaviour of mixtures like M0 was previously studied by Kandy et al. [26]. For Ca(OH)2 suspensions, they determined an increase in viscosity with rising temperatures. They explained this increase with a measured decrease of the zeta potential. The lower magnitude of the zeta potential leads to less repulsive electrostatic forces and thus increases the aggregation tendency. The temperature development of the storage modulus of M0 confirms this. The storage modulus increases of M2.5, M5 and M10 should follow a similar mechanism. The equilibrium between adsorbed and unabsorbed acrylic acid changes with temperature. Therefore, the amount of acrylic acid adsorbed on the calcium hydroxide particles changes with temperature as well. This should lead to a change in the magnitude of the zeta potential, which in turn should affect the rheological properties as described above. A measurement of the zeta potential of those suspension would help to deeper understand the observed phenomena. Especially the odd seeming decrease in storage modulus of M5 at 50°C is currently inexplicable.

Both M5 and M10 show a sharp increase of the storage modulus at 56°C and 62°C respectively. At this initiation temperature the thermal decomposition of the initiator VA-044 leads to the copolymerisation of acrylic acid and ethylene glycol dimethacrylate, drastically changing the rheology properties of the mixture. The observed initiation temperature is significantly higher than the 10-hour half-life decomposition temperature of VA-044 (44°C). The shift to a higher temperature can be explained by the high pH and high filler content, both factors strongly influencing the polymerization kinetics [27,28]. A similar increase in storage modulus through polymerization should occur for M2.5 but is not observable. The already high storage modulus of M2.5 before polymerization maybe masks the further increase.

In the last part of the heating ramp between 70°C and 80°C all suspensions reach a similar storage modulus. Especially M10 seems to reach a plateau at approx. 70°C. This could mean that the polymerization of acrylic acid is completed, and the suspension reached the maximum storage modulus. But at those high temperature water evaporation effects at the gap between the plates could also have a significant effect. Although silicon oil for gap sealing and a solvent evaporation trap was used, the similar storage modulus of all mixtures suggests that water evaporation at the gap between the plates dictates the storage modulus at temperatures above 70°C.

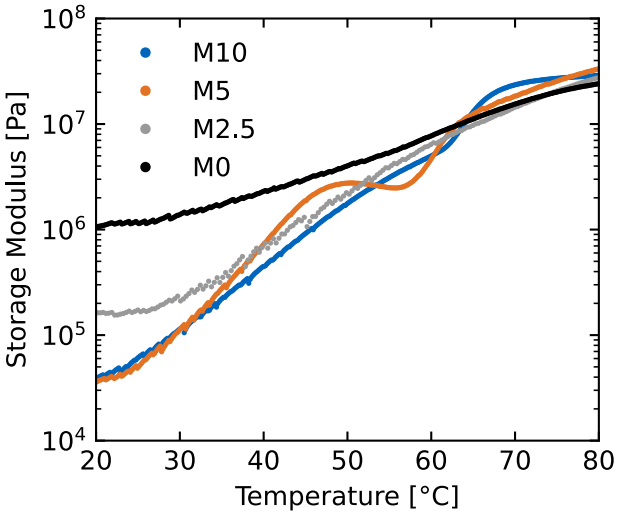

Figure 1 Development of the Storage Modulus (logarithmic) over temperature, measured by small angle oscillation rheometry, for M10, M5, M2.5 and M0.

2.2 Manufacturing of solid samples

To test the mechanical strength of the material after completion of the polymerization, we prepared small scale cuboid specimen using silicon moulds. As discussed in Chapter 2.1, the initiation temperature for polymerization is at approximately 60°C. Therefore, it was necessary to heat the moulds containing the paste. As the objective is to achieve a fast liquid to solid transition, we chose microwave heating to quickly heat up the samples. We tested two different heating protocols, either the mould was directly heated in the microwave (P1), or the mould was placed in a water bath (P2) like shown in Figure 2 and the entire setup i.e., water bath plus mould, was heated in the

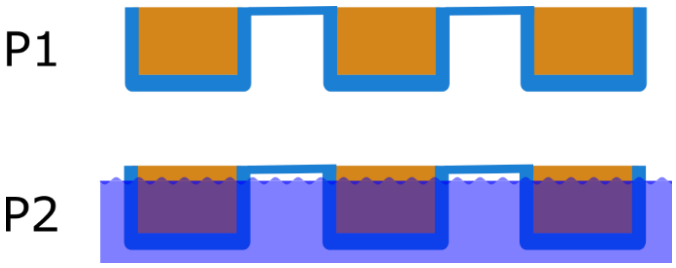

Figure 2 Scheme for the filled silicon mould for P1 (top) and P2 (bottom) partly submersed in a water bath.

microwave. P1 used a power setting of 1000 W for 10 seconds and P2 a power setting of 100 W for 10 minutes.

The visual impression of the rectangular cuboids after heating depends strongly on the microwave program. The high-power setting of P1 most likely leads to a very quick evaporation of water which made the cuboids lift out of the mould (Figure 3). Additionally, the evaporation of water and the vapor pressure led to the large cavities in the cuboids, as seen in Figure 4. P2, on the other side, had a significant longer microwave time but lead to well-shaped cuboids.

Figure 3 Silicon mould after microwave treatment with P1 (top) and P2 (bottom).

Figure 4 Demoulded cuboids (M10) for P1 (left) and P2 (right).

2.3 Compressive strength after polymerization

The microwave treatment also had a significant effect on the resulting compressive strength as shown in Figure 5.

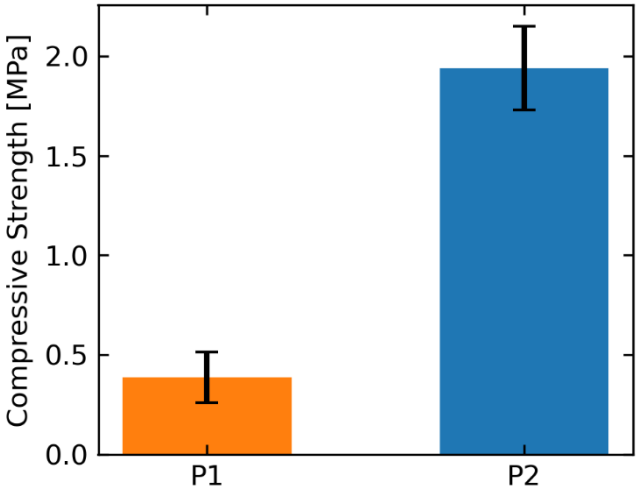

Figure 5 Comparison of the resulting compressive strength of paste M10 treated with P1 and P2.

The highly porous cuboids from P1 exhibit significantly reduced compressive strength compared to those obtained via P2. Further experiments were conducted using P2.

The samples M10, M5, M2.5 and M0 differ with respect to their polymer content. Not surprisingly, the variation of polymer content leads to differences in compressive strength of cuboids after heating (Figure 6), while the dimension and weight are comparable (Table 3). The polymer free sample M0 is missing in this comparison because the cuboids were too soft for testing. The polymer network formed by the in-situ polymerization probably adsorbs on multiple calcium hydroxide particles simultaneously, binding them together, thus creating cohesive forces. An increase in polymer content from M2.5 to M5 should therefore lead to more connecting bonds, resulting in stronger cohesive forces, apparent as an increase in compressive strength (Figure 6). Interestingly we don't see another significant increase in compressive strength from M5 to M10, although the polymer content is higher for M10. This suggest that no additional connecting bonds between particles were formed. This could, similar as discussed in section 2.1, be due to the saturation of the surface at 5 volume percentage polymers (M5).

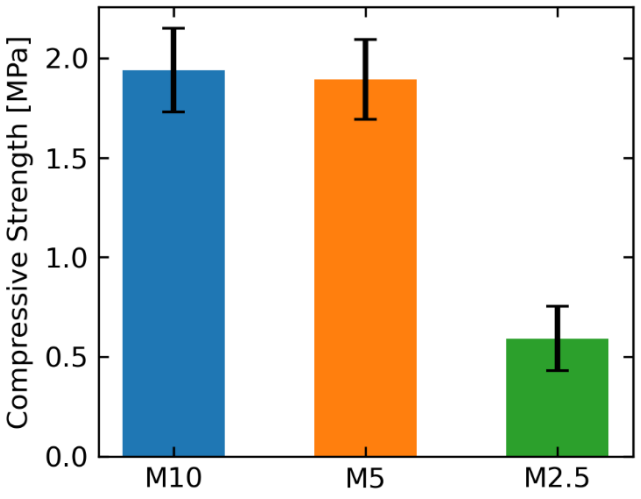

Figure 6 Compressive strength of M10, M5 and M2.5 after P2 treatment.

Table 3 Average dimension and weight, with standard deviation, of the tested cuboids (P2).

Mixture	M10	M5	M2.5
Width [mm]	9.78 (±0.07)	9.77 (±0.13)	9.36 (±0.15)
Length [mm]	15.77 (±0.07)	15.52 (±0.15)	15.55 (±0.09)
Height [mm]	15.89 (±0.16)	15.44 (±0.15)	15.58 (±0.08)
Mass [g]	3.361 (±0.048)	3.269 (±0.044)	3.213 (±0.051)
Density [kg m^{-3}]	1371	1396	1417

2.4 Compressive strength after storage

In a next set of experiments the compressive strengths of the cuboids after 1-, 3- and 7-days storage (at ambient conditions) were tested. Results are shown in figure 7. The increase of the mechanical strength is based on water evaporation and carbonation.

The decrease of water content through evaporation leads to cohesive capillary forces which are e.g., well studied for wet powders [29]. As seen in Figure 8 the mass loss trough the water evaporation is the dominant process for the first 37 hours leading to a compressive strength of 3.66 MPa after 24 hours.

After approx. 37 hours the carbonation of calcium hydroxide to calcium carbonate becomes apparent as mass gain. The carbonation of calcium hydroxide to calcite, through the available carbon dioxide in the atmosphere, leads to a positive change in mass of 220 mg (from hour 37 to 95). This is accompanied by a compressive strength increase from 1.94 MPa to 4.76 MPa. Since both processes happen at the same time it is not possible to evaluate the degree of carbonation by mass gain or quantify the strength increase of each process. In future experiments the humidity and caron dioxide content during carbonation will be controlled to separate those two processes and analyse them separately.

In the initial mix design M0 has a water content of 50 volume percentage (v%), even if we assume the unlikely full transformation of calcium hydroxide to calcium carbonate the water content is lowered to 48v%. After 7 days, most of the water should evaporate, leading to an approximate porosity of the cubes of 40v%. Studies on porous cementitious system usually don't cover such a high porosity but they deliver formulas to extrapolate their data. The exponential decrease of compressive strength with porosity described by Lian et. al. ($y=231.44e^{-0.9x}$) predicts a compressive strength of 6.32 MPa for a porosity of 40v%, whereas the liner correlation of Bhutta et al predicts negative values for such a high porosity [30,31]. The 4.76 MPa measured after 7 days of storage are at least comparable to the predicted 6.32 MPa, therefore the compressive strength of M10 could be comparable to concrete if the porosity is lowered significantly.

Figure 7 Compressive strength of M10 (prepared by P2) after 0, 1 ,3, 7 days.

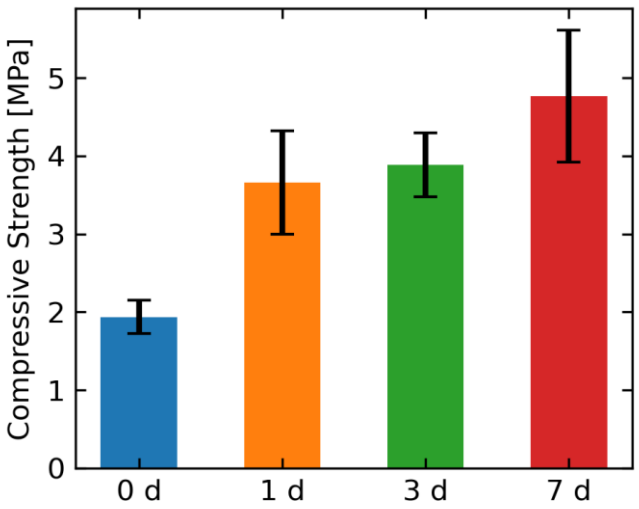

Table 4 Average dimension and weight, with standard deviation, of the aged cuboids (M10, P2).

Mixture	0 d	1 d	3 d	7 d
Width [mm]	9.78 (±0.07)	9.71 (±0.06)	9.91 (±0.20)	9.92 (±0.14)
Length [mm]	15.77 (±0.07)	15.69 (±0.07)	15.81 (±0.07)	15.67 (±0.16)
Height [mm]	15.89 (±0.16)	15.64 (±0.33)	15.79 (±0.14)	15.62 (±0.32)
Mass [g]	3.361 (±0.048)	2.462 (±0.022)	2.560 (±0.034)	2.550 (±0.038)
Density [kg m^{-3}]	1371	1033	1055	1050

Figure 8 Mass loss of 9 cuboids from M10 prepared by P2, measured with a balance.

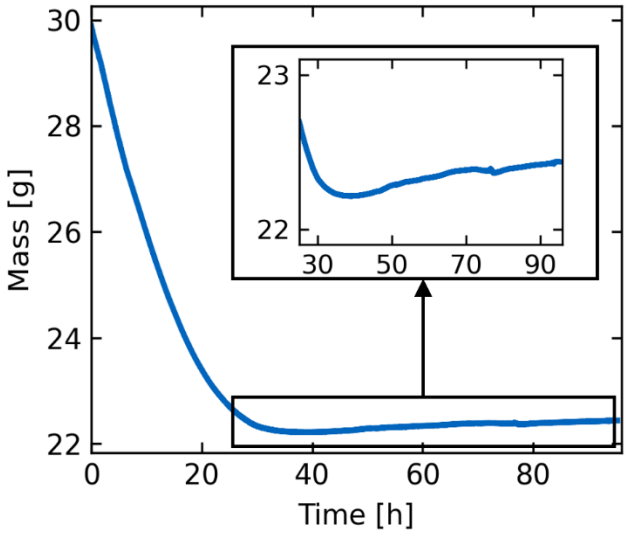

3 Conclusion

We demonstrate a hybrid binder system based on radical polymerization and carbonation which allows thermally controlled active stiffening control. The organic binder is a based on acrylic acid and an olefinic crosslinker. As soon as a thermally labile initiator molecule (an azo compound in our case) provides a sufficient flux of initiator radicals, the polymerization proceeds very rapidly and leads to a fast change in rheological properties and a build-up of mechanical strength. Depending on the heating program in the microwave a compressive strength of 0.39 MPa can be achieved in just 10 seconds or 1.94 MPa in 10 minutes. The final strength development was driven by water evaporation and the carbonation of calcium hydroxide. The combination of both processes leads to a compressive strength of 4.76 MPa after storing at ambient conditions for 7 days.

Compared to most conventual cementitious systems, the final mechanical strength of the present prototype is lacking and must be improved in further research. This will be achieved by an optimization of the carbonation process and a reduction of the porosity.

References

[1] G. De Schutter; K. Lesage; V. Mechtcherine; V.N. Nerella; G. Habert; I. Agusti-Juan (2018) *Vision of 3D printing with concrete — Technical, economic and environmental potentials*. Cem. Concr. Res., 112, 25–36. https://doi.org/10.1016/j.cemconres.2018.06.001

[2] F. Bos; R. Wolfs; Z. Ahmed; T. Salet (2016) *Additive manufacturing of concrete in construction: potentials and challenges of 3D concrete printing*. Virtual Phys. Prototyp., 11, 209–225. https://doi.org/10.1080/17452759.2016.1209867

[3] Y.W.D. Tay; B. Panda; S.C. Paul; N.A. Noor Mohamed; M.J. Tan; K.F. Leong (2017) *3D printing trends in building and construction industry: a review*. Virtual Phys. Prototyp., 12, 261–276. https://doi.org/10.1080/17452759.2017.1326724

[4] L. Reiter; T. Wangler; N. Roussel; R.J. Flatt (2018) *The role of early age structural build-up in digital fabrication with concrete*. Cem. Concr. Res., 112, 86–95. https://doi.org/10.1016/j.cemconres.2018.05.011

[5] L. Reiter; T. Wangler; A. Anton; R.J. Flatt (2020) *Setting on demand for digital concrete – Principles, measurements, chemistry, validation*. Cem. Concr. Res., 132, 106047. https://doi.org/10.1016/j.cemconres.2020.106047

[6] G. De Schutter; K. Lesage (2018) *Active control of properties of concrete: a (p)review*. Mater. Struct., 51, 123. https://doi.org/10.1617/s11527-018-1256-2

[7] N. Anandakrishnan; H. Ye; Z. Guo; Z. Chen; K.I. Mentkowski; J.K. Lang; N. Rajabian; S.T. Andreadis; Z. Ma; J.A. Spernyak; J.F. Lovell; D. Wang; J. Xia; C. Zhou; R. Zhao (2021) *Fast Stereolithography Printing of Large-Scale Biocompatible Hydrogel Models*. Adv. Healthc. Mater., 10, 2002103. https://doi.org/10.1002/adhm.202002103

[8] M.P. Lee; G.J.T. Cooper; T. Hinkley; G.M. Gibson; M.J. Padgett; L. Cronin (2015) *Development of a 3D printer using scanning projection stereolithography*. Sci. Rep., 5, 9875. https://doi.org/10.1038/srep09875

[9] H. Song; N.A. Rodriguez; C.C. Seepersad; R.H. Crawford; M. Chen; E.B. Duoss (2021) *Development of a variable tensioning system to reduce separation force in large scale stereolithography*. Addit. Manuf., 38, 101816. https://doi.org/10.1016/j.addma.2020.101816

[10] D. Moreno Nieto; S.I. Molina (2020) *Large-format fused deposition additive manufacturing: a review*. Rapid Prototyp. J., 26, 793–799. https://doi.org/10.1108/RPJ-05-2018-0126

[11] N. Volpato; D. Kretschek; J.A. Foggiatto; C.M. Gomez da Silva Cruz (2015) *Experimental analysis of an extrusion system for additive manufacturing based on polymer pellets*. Int. J. Adv. Manuf. Technol., 81, 1519–1531. https://doi.org/10.1007/s00170-015-7300-2

[12] T. Ebert; A. Seifert; S. Spange (2015) *Twin Polymerization—a New Principle for Hybrid Material Synthesis*. Macromol. Rapid Commun., 36, 1623–1639. https://doi.org/10.1002/marc.201500182

[13] G. Kickelbick (2004) *Hybrid Inorganic–Organic Mesoporous Materials*. Angew. Chem. Int. Ed., 43, 3102–3104. https://doi.org/10.1002/anie.200301751

[14] F. Ribot; C. Sanchez (1999) *Organically Functionalized Metallic Oxo-Clusters: Structurally Well-Defined Nanobuilding Blocks for the Design of Hybrid Organic-Inorganic Materials*. Comments Inorg. Chem., 20, 327–371. https://doi.org/10.1080/02603599908021449

[15] M.I. Sarwar; Z. Ahmad (2000) *Interphase bonding in organic–inorganic hybrid materials using aminophenyltrimethoxysilane*. Eur. Polym. J., 36, 89–94. https://doi.org/10.1016/S0014-3057(99)00046-4

[16] A. Jenni; L. Holzer; R. Zurbriggen; M. Herwegh (2005) *Influence of polymers on microstructure and adhesive strength of cementitious tile adhesive mortars*. Cem. Concr. Res., 35, 35–50. https://doi.org/10.1016/j.cemconres.2004.06.039

[17] S. Donatello; M. Tyrer; C.R. Cheeseman (2009) *Recent developments in macro-defect-free (MDF) cements*. Constr. Build. Mater., 23, 1761–1767. https://doi.org/10.1016/j.conbuildmat.2008.09.001

[18] R. Liang; Q. Liu; D. Hou; Z. Li; G. Sun (2022) *Flexural strength enhancement of cement paste through monomer incorporation and in situ bond formation*. Cem. Concr. Res., 152, 106675. https://doi.org/10.1016/j.cemconres.2021.106675

[19] S. Bhagavathi Kandy; I. Mehdipour; N. Neithalath; A. Kumar; M. Bauchy; E. Garboczi; S. Srivastava; T. Gaedt; G. Sant (2022) *Ultrafast stiffening of concentrated thermoresponsive mineral suspensions*. Mater. Des., 221, 110905. https://doi.org/10.1016/j.matdes.2022.110905

[20] K. Matyjaszewski; T.P. Davis, eds. (2002) Handbook of radical polymerization Wiley-Interscience - Hoboken.

[21] L. Brocken; P.D. Price; J. Whittaker; I.R. Baxendale (2017) *Continuous flow synthesis of poly(acrylic acid) via free radical polymerisation*. React. Chem. Eng., 2, 662–668. https://doi.org/10.1039/C7RE00063D

[22] N. Koga; K. Tsuru; I. Takahashi; K. Ishikawa (2015) *Effects of humidity on calcite block fabrication using calcium hydroxide compact*. Ceram. Int., 41, 9482–9487. https://doi.org/10.1016/j.ceramint.2015.04.005

[23] S. Matsuya; X. Lin; K. Udoh; M. Nakagawa; R. Shimogoryo; Y. Terada; K. Ishikawa (2007) *Fabrication of porous low crystalline calcite block by carbonation of calcium hydroxide compact*. J. Mater. Sci. Mater. Med., 18, 1361–1367. https://doi.org/10.1007/s10856-007-0123-4

[24] A. Otsu; K. Tsuru; M. Maruta; M.L. Munar; S. Matsuya; K. Ishikawa (2012) *Fabrication of microporous calcite block from calcium hydroxide compact under carbon dioxide atmosphere at high temperature*. Dent. Mater. J., 31, 593–600. https://doi.org/10.4012/dmj.2011-252

[25] S.B. Johnson; G.V. Franks; P.J. Scales; D.V. Boger; T.W. Healy (2000) *Surface chemistry–rheology relationships in concentrated mineral suspensions*. Int. J. Miner. Process., 58, 267–304. https://doi.org/10.1016/S0301-7516(99)00041-1

[26] S. Bhagavathi Kandy; I. Mehdipour; N. Neithalath; M. Bauchy; E. Garboczi; S. Srivastava; T. Gaedt; G. Sant (2020) *Temperature-Induced Aggregation in Portlandite Suspensions*. Langmuir, 36, 10811–10821. https://doi.org/10.1021/acs.langmuir.0c01798

[27] V.A. Kabanov; D.A. Topchiev; T.M. Karaputadze (1973) *Some features of radical polymerization of acrylic and methacrylic acid salts in aqueous solutions*. J. Polym. Sci. Polym. Symp., 42, 173–183. https://doi.org/10.1002/polc.5070420120

[28] S.H. McGee (1982) *Curing characteristics of particulate-filled thermosets*. Polym. Eng. Sci., 22, 484–491. https://doi.org/10.1002/pen.760220806

[29] A. Goldszal; J. Bousquet (2001) *Wet agglomeration of powders: from physics toward process optimization*. Powder Technol., 117, 221–231. https://doi.org/10.1016/S0032-5910(00)00369-7

[30] C. Lian; Y. Zhuge; S. Beecham (2011) *The relationship between porosity and strength for porous concrete*. Constr. Build. Mater., 25, 4294–4298. https://doi.org/10.1016/j.conbuildmat.2011.05.005

[31] M.A.R. Bhutta; K. Tsuruta; J. Mirza (2012) *Evaluation of high-performance porous concrete properties*. Constr. Build. Mater., 31, 67–73. https://doi.org/10.1016/j.conbuildmat.2011.12.024